Modelling of the hydro-acoustic signal as a Tsunami Precursor

Francesco Chierici

Istituto di Radioastronomia, Istituto Nazionale di Astrofisica, sez. Bologna,

via Gobetti, 101 - 40129 Bologna, Italy

Luca Pignagnoli

Istituto di Scienze Marine, Consiglio Nazionale delle Ricerca, sez. Bologna,

via Gobetti, 101 - 40129 Bologna, Italy

Davide Embriaco

Istituto Nazionale di Geofisica e Vulcanologia, sezione Roma 2, via Pezzino

Basso, 2 - 19025 Portovenere (SP), Italy

F. Chierici, IRA-INAF (chierici@ira.inaf.it)

Abstract. In the frame of a 2-D compressible tsunami generation model with flat porous seabed, we show that acoustic waves are generated and travel outside the source area at sound speed. These waves carry information as to sea floor motion. The acoustic wave period depends on water height at the source area and is given by four times the travel time the sound takes to reach the sea surface from the sea bottom. The fundamental frequency ranges from 1 to 0.05 Hz, at 400 m and 8000 m water depth, respectively. The sound waves produced by seafloor motion can propagate far from the source, with a small attenuation in amplitude. Moreover, the typical wavelengths of the acoustic waves produced by the water layer oscillation allows the waves to overcome most of the seafloor reliefs. The semi-analytical solution of the 2-D compressible water layer model overlying a porous seabed is presented.

1. Introduction

Tsunami waves, which travel long distances at speeds depending on water depth, can be very dangerous and destructive, as shown by the recent as well as disastrous Sumatra earthquake (*Lomnitz and Nilsen-Hofseth* [2005], *Merrifield et al.* [2005]). Tsunamis can be generated by a number of different mechanisms, such as shallow-depth submarine earthquakes, sub-aerial and submarine landslides or volcanic eruptions and consequent submarine landslides (*Synolakis et al.* [2002] , *Tinti et al.* [2004]), meteoric impacts or sudden and large barometric variations at sea (i.e. storm surges). The most common and effective mechanism is the earthquake, as reported by historical sources (*Boschi et al.* [1997] , *Tinti et al.* [2004] , NGDC Tsunami Catalog [@]).

Starting from 1980s, many different theoretical approaches, both analytical (*Ward* [1980], *Comer* [1984], *Okal* [1988], *Panza et al.* [2000]) and numerical (*Titov et al.* [2005], *Kowalik et al.* [2005]), have been developed to model tsunami generation. Most of these studies take into account a wide variety of physical characteristics within the framework of incompressible fluid theory with just a few exceptions (e.g. *Nosov* [1999], *Ohmachi et al.* [2001]). These theoretical approaches are mainly based on an elastic half-space coupled with an incompressible water layer on a spherical domain (*Ward* [1980], *Ward* [1981], *Ward* [1982]) or in a plane domain (*Comer* [1984]) or coupled with a stratified incompressible fluid (*Panza et al.* [2000]). Recently, some authors have accounted for the relevant role played by water compressibility in tsunami generation, in particular showing that the compressibility is relevant only in the generation phase and not in the propagation (*Nosov* [1999], *Nosov and Skachko* [2002], *Nosov and Kolesov* [2007]). The general contribution of compressibility in tsunami evolution was presented in the works of (*Miyoshi* [1954], *Sells* [1965], *Kajiura* [1970]). The assumption of the local compressibility of the water layer allows the sound waves, that is pressure waves, to form and propagate into the water layer.

The first convincing experimental proof of the existence of elastic waves generated in the fluid by a bottom motion with frequency inversely proportional to the water depth was obtained during the Tokachi-Oki 2003 tsunami event, when the real-time JAMSTEC observatory detected the acoustic pressure signal, with 0.05 Hz frequency generated by the seafloor motion caused by the earthquake (*Nosov et al.* [2007], *Nosov and Kolesov* [2007]). The two pressure sensors operated by JAMSTEC were located in the epicentre area, allowing for a direct measurement of water pressure variation during the earthquake.

In spite of the great scientific and technological effort made to deal with the tsunami hazard over the past few years and in spite of the numerous studies performed on tsunamigenic sources (e.g. *Synolakis et al.* [1997], *Ma et al.* [1997], *Zitellini et al.* [1999], *Baptista et al.* [2003]), propagation and flooding of tsunami waves (*Synolakis* [1995], *Titov et al.* [2005]), the details of tsunami generation processes are still poorly understood, mainly because of the scarcity of direct measurements in tsunami generation areas.

We present a simple model, which by taking account of local water compressibility and porous seabed, signals the important characteristics of tsunami generation processes that can enhance the present tsunami warning capability (DART project [@], DONET project [@], GITEWS project [@], NEAREST project [@], TRANSFER project [@]) and the understanding of the source ground motion.

2. Model

We have developed a new 2-D model with a compressible water layer overlying a porous sea bottom, which we solved semi-analytically (*Nosov* [1999], *Nosov and Skachko* [2001], *Nosov and Skachko* [2002], *Gu and Wang* [1991], *Habel and Bagtzoglou* [2005]). We assumed the approximation of small-amplitude waves that allows us to simplify the model to a linear problem. In particular, by introducing a boundary condition that equals the vertical component of the fluid velocity and the pressure at the water-sediment interface, we estimated the pressure field in the vicinity of the seafloor generated by the fluid escape from the sediment, caused by the "earthquake".

In this paper we have omitted to show the solution of the pressure field in the sediment layer and the results of the high number of numerical simulations we ran with the different kinds of seafloor motions implemented, i.e. many different elastic motions, with different initial polarity, amplitudes, phases, durations, combined with different permanent displacements and with different parameters. Nor have we presented the pressure and the velocity field maps computed, both in the fluid and in the porous layers. We have postponed a complete presentation of these results to a future paper.

We have focused only on some aspects of the outputs of the simulations concerning hydro-acoustic signal, which for sake of simplicity and brevity, are better illustrated by showing the solution in the water layer and for permanent displacement.

The Navier-Stokes equation is the governing equation in the water layer, while in the porous layer we used the Darcy equation. The Navier-Stokes equation is:

$$\begin{cases} \frac{\partial \rho}{\partial t} + \nabla \cdot (\rho \mathbf{u}) = 0 \\ \frac{\partial \vec{U}}{\partial t} + \vec{U} \cdot \nabla \vec{U} = -\frac{1}{\rho} \nabla P - \vec{g} + \nu \nabla^2 \vec{U} \end{cases} \quad (1)$$

The Darcy equation is:

$$\begin{cases} \nabla \cdot \vec{Q} = 0 \\ \\ \nabla P_s = \frac{\mu}{K_p}\vec{Q} + \frac{\rho}{n}\frac{\partial \vec{Q}}{\partial t} \end{cases} \tag{2}$$

where in eq. (1) ρ is the fluid density (set equal to 1020 Kg/m^3), $\vec{U}$ the fluid velocity, P the pressure, ν the kinematic viscosity (set equal to 2 $\times 10^{-6}$m^2/s), and g the gravity acceleration.

In the Darcy eq. (2) $\vec{Q} = (Q_x, Q_z)$ is the discharge velocity, P_s the pore pressure, K_p and n the intrinsic permeability and volumetric porosity, respectively, $\mu = \nu\rho$ the fluid dynamic viscosity.

We have introduced some simplifying assumptions to solve the model analytically. In particular, the small-amplitude-wave approximation, i.e. a wave amplitude small with respect to its wavelength, that is satisfied also by huge tsunami waves in the open ocean, and the non-viscous fluid approximation in the water layer (viscosity is not significant at typical tsunami scales):

$$\frac{A}{\lambda} \ll 1 \tag{3}$$

$$\nu = 0 \Rightarrow \vec{U} = \nabla \varphi \tag{4}$$

where A is the wave amplitude, λ is the wavelength and φ is the potential field. Applying these approximations we obtained:

$$\nabla^2 \varphi = \frac{1}{c^2}\frac{\partial^2 \varphi}{\partial t^2} \tag{5}$$

$$P = -\rho\frac{\partial \varphi}{\partial t} - \rho g z \tag{6}$$

where c is the sound velocity in the water (about 1500 m/sec, depending on sea water temperature and salinity), and z the vertical upwards direction.

The boundary conditions at free surface ($z = 0$) are

$$\frac{\partial \varphi}{\partial t} = -g\xi \Big|_{z=0} \tag{7}$$

$$\frac{\partial \xi}{\partial t} = \frac{\partial \varphi}{\partial z} \Big|_{z=0} \tag{8}$$

that represent the dynamic and the kinematic conditions, respectively, ξ is the free surface perturbation.

The boundary conditions at the water-sediment interface ($z = -h$) are

$$\rho \frac{\partial \varphi}{\partial t} = P_s \Big|_{z=-h} \tag{9}$$

$$\frac{\partial \varphi}{\partial z} = Q_z \Big|_{z=-h} \tag{10}$$

that represent the continuity of the stress field and of the vertical component of the fluid velocity, respectively.

We assumed the non-permeability of the sea bottom underlying the porous sedimentary layer: the boundary condition at the bottom of the porous sedimentary layer ($z = -(h + h_s)$) is given by:

$$Q_z = \frac{\partial \eta}{\partial t} \Big|_{z=-(h+h_s)} \tag{11}$$

where $\eta(x, t)$ is the bottom motion. The small-amplitude approximation, i.e. $\eta/h \ll 1$, must be satisfied.

We solved the equations by obtaining the potential field and the pressure in the porous layer by Fourier transforming with respect to x and Laplace transforming with respect to the time t:

$$\varphi(x, z, t) = \frac{1}{4\pi^2 i} \int_{s-i\infty}^{s+i\infty} d\omega \int_{-\infty}^{+\infty} dk \, [A(k, \omega)\sinh(-\alpha z) + B(k, \omega)\cosh(-\alpha z)] e^{\omega t + ikx} \tag{12}$$

$$P_s(x,z,t) = \frac{1}{4\pi^2 i}\int_{s-i\infty}^{s+i\infty} d\omega \int_{-\infty}^{+\infty} dk\,[C(k,\omega)\sinh(-kz) + D(k,\omega)\cosh(-kz)]e^{\omega t+ikx} \quad (13)$$

from which the desired quantities can be computed by using (4), (6) and (7). The A, B and α expressions are given in Appendix A, while the solution within the porous medium (C and D) is not given here.

3. Results

The solved model allows us to study the signal amplitude and shape in the water layer at different distances and depths, for different bottom motions. In this paper we have only presented a simple kind of motion, i.e. the piston-like motion caused by a seabed displacement of fixed length $2a$, which rises at constant velocity v_B, reaching the final permanent elevation η_0 in time τ (permanent displacement). We have computed far more complicated motions by combining this basic motion with a time shift operation (see Appendix B) to obtain, for instance, an elastic seafloor motion with many different superimposed frequencies whether followed or not by permanent displacement. On the other hand, the contribution of different piston-like motions with different lengths, amplitudes, phases, durations, polarities and time shifts has been investigated.

As a consequence of model linearity, it can be shown that all the output parameters (i.e. sea level displacement ξ, the pressure P, etc.) are proportional to seafloor motion amplitude η_0. The indicative value of η_0=1m for the amplitude of the vertical displacement has been used.

In Fig. 1 the water surface at different observation points is shown, given a positive permanent displacement of the sea bottom of 25-s duration. The displacement length is chosen at $2a$=60 km with a 3000 m water depth. The observing points are located at $\bar{x}$=

100, 200, 300 and 1000 km from the source, respectively. A 1500 m-thick porous seabed, with volumetric porosity n=0.3, and a permeability $K_p = 10^{-6}$ cm^2, is assumed.

In Fig. 2 is shown the same simulations of Fig. 1, with the same parameters except for the observation point, chosen at 1500 m depth. In the latter case, the vertical axis unit is given in hPascal, roughly corresponding to 1 cm of equivalent water height, to favour a direct comparison between the two simulations.

In both cases the signal amplitude decreases with the distance as $\bar{x}^{-1/2}$, showing small attenuation amplitude also at a long distance from the source. The two Figures clearly show the acoustic signal and its modulation, induced in the compressible water layer by the seafloor motion. The signal vibrates at frequencies $\nu_l = c(2l+1)/4h$, where h is the water depth and $l = 0, 1, 2, \ldots$ (*Nosov* [1999]). The acoustic signal travels at sound speed c (here assumed equal to 1500 m/s), and reaches the observing points at time $t_s = \bar{x}/c$ ($\bar{x}$=100, 200, 300, 1000km), well preceding the arrival of the tsunami wave, which travels at a lower speed $v_T = (gh)^{1/2}$. There is a shape difference between the signal modulation at the water surface and the signal modulation in depth, described by the function $f_p(k, \omega, z)$ in the (k, ω) domain (see Appendix A), which acts as a sort of transfer function.

An interesting feature of the soundwave emitted by the compressible water layer oscillation, excited by the sea bottom motion, is its amplitude modulation. This acoustic modulation carries information about seafloor motion and geometry.

In Fig. 3 the variation of the wave amplitude versus the source length (chosen as $2a$=30, 60, 90 km respectively) is shown. The same bottom displacement is used as in Figs.1 and 2, at an observation distance of 300 km in a 1500 m-thick water layer with a 750 m sedimentary bottom, for a 1 s motion duration. Permeability and porosity are the same as in the previous simulations.

The envelopes can be obtained by applying a demodulation technique to the signals of Fig. 3, as a Hilbert transform or the "square and low pass". It is easy to see that the number of modulation packets (pulses) is proportional to the ratio among the source lengths: as the length of the source increases the number of modulations packets within a time-interval increases by the same ratio. Furthermore, the mean slopes of the pulses scales proportionally with the source lengths; the mean slope has been defined as the difference between the relative maximum pulse and its relative minimum divided by the pulse semi-length. The mean slope of the pulses varies with the energy released by the bottom motion into the water layer due to different source lengths. As shown by Nosov (*Nosov* [1999], *Nosov et al.* [2007], *Nosov and Kolesov* [2007]), within the frame of a compressible model the energy transmitted to the water layer by the bottom motion is given by $W = \rho c V^2 S \tau$. While tsunami energy, computed in the approximation of incompressible fluid, is roughly given by $W_T = 0.5 \rho g S (V\tau)^2$, where S is the source area, V the sea bottom velocity and τ the duration of the motion. Taking into account that the bottom velocity is given by $V = \eta_0/\tau$, where η_0 is amplitude of the ground motion, and substituting S with L for a source in the 2-D model, we can rewrite $W = \rho c V L \eta_0$. It is straightforward to argue that if the mean slope is effectively an indicator of the energy released by the bottom motion into the water layer and it scales proportionally to the source length (see Fig. 3), it should also scale proportionally to the bottom velocity.

Fig. 4 shows the modulated acoustic waves caused by the same seafloor motion as in Fig. 3, but with different velocities v_B of the source (here with a fixed length of $2a$=30 km), which reaches the observation point located at a distance of $\bar{x}$=300 km from the tsunami source. All the other parameters, such as water depth, porosity, etc., are the same as in the previous cases. Apart from the different amplitudes, the modulations appear to be quite similar. The mean slope of the envelopes scales with the same ratio of the different velocities as expected.

Summarizing, by using a semi-empirical approach to the data interpretation, we showed that within the acoustic modulation there is information of the source length, the ground motion velocity and amplitude, and the water depth at the source location. This information can be extracted; in fact the source velocity, length and amplitude η_0 can be calibrated taking into account the fact that the source distance, the duration of the motion and the earthquake moment can, for instance, be independently retrieved from the seismic network.

A tsunami is always produced if a permanent seafloor displacement occurs. In principle, within the framework of the model, by using the characteristics of the acoustic waves propagating into the water layer and the equations of continuous mechanics in the approximation of an elastic half-plane (again if the distance from the source and the earthquake magnitude are independently known) we can estimate the stress field at the source to evaluate the possible seafloor rupture; in this sense, the acoustic signal can be considered a tsunami precursor.

In Figs. 5 and 6 the effect due to the interference between the frequency of ground motion and the fundamental frequency of oscillation of the water column is shown. In this case a 1500 m water depth (the proper frequency of the water layer is 0.25 Hz and we use this frequency and its harmonics for the bottom motion), a 750 m sediment thickness, a 30 km source length and an observation point at 375 km from the source have been used. As can easily be seen, the shape of the modulation in the ”resonant” case is quite different from the modulation produced by ground motions with periods different from the period of the fundamental oscillation of the water column. Moreover, the amplitude of the ”resonant” signal is much smaller than the ”non-resonant” one (see Figs. 1, 2, 3). The permanent displacement ”resonant” modulation presents a typical and clearly recognizable feature with respect to the ”non-resonant” one, and scales monotonically with the seafloor velocity as demonstrated by looking at the envelopes and at Fig. 5 that again shows a linear relationship among the mean slopes and the bottom velocities with correlation coefficient r^2=0.9987. After a first-pulse train, which scales proportionally to the velocities, the modulations turn into tails where the magnitude of the signals is almost the same for any ”resonant velocity” before the tsunami arrives. Differences are in the order 10^{-3} times the signal amplitude values. The very first part of the demodulation must be discharged in this particular case because the low pass filter demodulation technique fails in tightly follow the first high frequency pulses, due to the filter parameters settings. On the contrary, the tsunami wave amplitude is not affected by this sort of interference (see Fig. 9). The features of ”resonant” acoustic signal is clearly recognizable from the non-resonant one, both from the signal pattern as well as from power spectra. The interference due to the same period of the seafloor motion and of the seawater-layer fundamental oscillation does not erase the source parameter information carried by the acoustic signal. This result remains valid also for much more complicated motions (see Appendix B). The information about the source parameters is contained in the acoustic modulation and can be retrieved.

In Fig 7 the acoustic modulation produced by a bottom motion with period far from resonance is shown for pattern comparison (the observation point is placed at same distance of 375km from the source).

In Fig. 8 the spectra of "resonant" and "non-resonant" modulations are shown. Both spectra are peaked at the fundamental frequency of the water layer. Odd harmonics are also present. The "resonance" spectrum is characterised by a lower amplitude of the peaks, but a much more distributed power.

In Fig. 9 an example of tsunami generated by a permanent displacement bottom motion with 4 s "resonant period " is shown. The observing distance is 100 km from the source. The other parameters are the same used in Fig. 1.

Finally, in Fig. 10 the comparison between the compressible water layer perturbation with or without taking into a account the porous bottom effect is shown. The presented model reduces to the Nosov's compressible model, in the limit of null-sediment thickness. The main effect of the porous layer is a lowering of the signal amplitude, during both generation and propagation, and also a high frequency smoothing. Fig. 10 (b) shows the comparison between the outputs of the compressible model with or without a porous bottom: by introducing the sediment effect the signal amplitude is damped. To magnify the effect here a porosity of 0.5 and a 1800 m sediment thickness were used. In Figs. 10 (c) and (d) the comparison between the corresponding power spectra is shown. The porous layer causes a cut-off effect on the high frequencies as can be seen in Figure 10 (d). The tsunami wave height is also influenced by the presence of a porous bottom that causes a small reduction of the wave amplitude.

4. Discussion

Some results of a 2-D semi-analytical model for tsunami generation have been presented in the case of "piston-like" motion with residual permanent displacement, also taking into account local water compressibility and seabed porosity. In Appendix B we show that much more complicated sea-bottom motions can be obtained by combining the piston-like motion and the time-shift operator. Hence, the results obtained for the permanent displacement are still valid for these motions. In appendix A it is proven that the acoustic modulation obtained at depth can be always related to an equivalent acoustic modulation at the free surface.

Attention has to be paid to the interpretation of the results obtained for many different reasons. The model is a simplified representation in respect to the real ocean. Moreover, this work uses a flat bottom 2-D model that neither takes into account possible interference effects due to a 3-D wave generation and the bathymetric gradients nor eventual signal masking due to the environmental noise. Also the contribution of the non linear effects during the generation process is not taken into account (*Nosov and Skachko* [2001, 2002]). Nevertheless, the acoustic signal generated by the ground motion shows relevant features directly related to the distance, extension, velocity, amplitude, frequency and water-column height at the source. These characteristics are still present in the acoustic signal generated by more complicated seafloor motion (see Appendix B). The sea bottom motion always generates acoustic waves in the water layer, but the presence of acoustic signals within the water column is not in itself an indicator of a tsunami wave. In fact, only residual seafloor displacement definitely generates tsunami, while elastic seafloor motion may generate a tsunami depending on the motion frequency and on the water-column height (*Nosov* [1999]; *Nosov and Kolesov* [2007]). Nevertheless, by knowing the distance from the source and the earthquake magnitude, the information about the extension, the velocity and the amplitude of the ground motion at the source can be recovered from the modulation. In turn this information allows us to infer whether a seafloor rupture has been probably produced or not with a residual displacement. In this sense, the acoustic modulation can be considered as a tsunami precursor.

The method we devised to extract information on the modulation has to be understood as an heuristic method. It is important to underline that the distance from the source and the earthquake magnitude are parameters that can be acquired from the data collected by the seismic networks.

The existence of acoustic waves generated by seafloor motion in the actual oceanic environment is demonstrated by the in-situ measurements performed by the real-time JAMSTEC observatory during the Tokachi-Oki-2003 earthquake and consequent tsunami. The spectral analysis of the water pressure records clearly shows the low-frequency elastic oscillation of the water column (*Nosov et al.* [2007]; *Nosov and Kolesov* [2007]) expected and predicted by the compressible fluid formulation. The paper on the Tokachi-Oki event is also a good example of how much attention has to be paid in the application of model results to the actual environment. As expected from the theory, the elastic oscillation carries information on the water-column height at the source (7500 m in the Tokachi-Oki area), and also shows other frequency components that are much harder to interpret.

5. Conclusions

Some remarkable characteristics can be extracted from the acoustic signal generated in the water layer by the seafloor motion by applying a semi-empirical approach to the outputs of a number of simulations:

1. the acoustic signal generated by the sea-floor motion travels from the source at sound speed, reaching the observation points much earlier than the possible tsunami wave, also in case of occurrence in very deep waters;

2. the acoustic signal shows a low attenuation in amplitude also at a long distance from the source;

3. the amplitude of the acoustic signal scales with $\bar{x}^{-1/2}$ where $\bar{x}$ is the observing point-source distance;

4. the number of modulation packets, the amplitude of the acoustic signal and the mean slope of the pulse scale with the source length;

5. the acoustic signal carries information on sea bottom velocity and water depth at the source;

6. "resonance" interference between the bottom motion and the elastic proper frequency of the water layer does not clear the source motion information contained in the acoustic signal;

7. the main effect of the porosity is a low-pass filtering of the signals and a damping of the tsunami wave amplitude and the acoustic modulation.

In conclusion, the pulses of the acoustic envelope carry a surprising amount of information as to the source parameters, the source bottom motion, and the energy that the ground motion releases to the water column. This information may allow for the development of a tsunami-warning technique based on this acoustic precursor and gives outstanding information as to source ground motion. To apply these conclusions to the ocean itself will require a great deal of work on the theoretical as well as the experimental sides.

Appendix A: Relationship between Inner Pressure and Free Surface

Some details on the solution of the equation of motion within the water layer, see eq. (12), are here reported, while the explicit solution for the porous sediment layer is not given. In particular, solving equations (2) and (5), in the Laplace and Fourier space and imposing the boundary conditions, the problem reduces to a linear system of four equations in the four variable $A(k,\omega)$, $B(k,\omega)$, $C(k,\omega)$, $D(k,\omega)$. The first two defining the pressure field into the water column, while the other two define the pressure field within the porous sediment layer. Moreover, using the linear de-convolution algorithm, it is possible to reconstruct the free-surface signal starting from the pressure signal within the water layer, evaluated at a fixed depth z_0.

The functions $A(k,\omega)$ and $B(k,\omega)$, used in eq. (12), are defined as:

$$A = \frac{\omega^2}{g\alpha} B \tag{A1}$$

$$B = -2\mu_p(\omega)\omega \frac{\sinh(kh)}{\cosh[k(h+h_s)]} \frac{\psi}{A_s(k,\omega)\sinh(\alpha h) + A_c(k,\omega)\cosh(\alpha h)} \tag{A2}$$

The functions $C(k,\omega)$ and $D(k,\omega)$ describing the pressure field into the porous domain (that are not presented here) can be derived from $A(k,\omega)$ and $B(k,\omega)$.

The symbols used in $A(k,\omega)$ and $B(k,\omega)$ are defined as:

$$\mu_p(\omega) = \frac{\mu}{K_p} + \frac{\rho\omega}{n} \tag{A3}$$

$$\alpha^2 = k^2 + \frac{\omega^2}{c^2} \tag{A4}$$

$$A_s(k,\omega) = \frac{2k\rho\omega^3}{\alpha g}[1 - \cosh^2(kh)t_h(k)] + \mu_p(\omega)\alpha\sinh(2kh)t_h(k) \tag{A5}$$

$$A_c(k,\omega) = 2k\rho\omega[1 - \cosh^2(kh)t_h(k)] + \frac{\mu_p(\omega)\omega^2}{g}\sinh(2kh)t_h(k) \tag{A6}$$

$$t_h(k) = 1 - \tanh(kh)\tanh[k(h+h_s)] \tag{A7}$$

$\psi(k,\omega)$ is the Laplace (time) and Fourier (x space coordinate) transform of the bottom floor motion $\eta(x,t)$:

$$\eta(x,t) = \frac{1}{2\pi i}\int_{s-i\infty}^{s+i\infty} d\omega \Big[\frac{1}{2\pi}\int_{-\infty}^{+\infty} dk\ \psi(k,\omega)e^{\omega t + ikx}\Big] \tag{A8}$$

The permanent displacement is described by the function:

$$\eta(x,t) = \eta_0[\theta(x+a) - \theta(x-a)]\Big[\frac{\theta(t)t - \theta(t-\tau)(t-\tau)}{\tau}\Big] \tag{A9}$$

Where θ is the Heaviside function.

The pressure fluctuations within the water column, at depth z, can be obtained using eq. (6):

$$P(x,z,t) = -\rho \frac{1}{4\pi^2 i} \int_{s-i\infty}^{s+i\infty} d\omega \int_{-\infty}^{+\infty} dk\, \omega f_p(k,\omega,z) B(k,\omega) e^{\omega t + ikx} \tag{A10}$$

where:

$$f_p(k,\omega,z) = \frac{\omega^2}{g\alpha} \sinh(-\alpha z) + \cosh(-\alpha z) \tag{A11}$$

The free-surface elevation, that can be obtained using eq. (7), is similar to the previous expression given for pressure field, except for the multiplying integrand factor $f_p(k,\omega,z)$. In fact:

$$\xi(x,t) = -\frac{1}{g} \frac{1}{4\pi^2 i} \int_{s-i\infty}^{s+i\infty} d\omega \int_{-\infty}^{+\infty} dk\, \omega B(k,\omega) e^{\omega t + ikx} \tag{A12}$$

Using the properties of the Laplace and Fourier transforms, the pressure field at depth, given by equation (A10), can be obtained from the linear convolution between the free-surface perturbation, given by equation (A12), and the inverse Laplace and Fourier transforms of the function $f_p(k,\omega,z)$. In other word, the source information carried in the free-surface modulation is still present at depth and can be recovered applying a linear de-convolution.

Appendix B: Composition of motion

In the case of seafloor motion with final permanent displacement, the free-surface solution, evaluated at fixed location $\bar{x}$, carries on relevant information concerning the source motion and geometry. Different and more complicated sea bottom motions can be obtained combining the permanent displacements with time-shift operations. The free-surface solution, corresponding to these different motions, can be related to the solution obtained for the permanent displacement, moreover it can be inverted using the Laplace transform and its properties. As a consequence, also in the case of more complicated seafloor motions, the acoustic modulation still carries on the same information about the source motion and geometry. In Fig. (11) some examples of seafloor motions are displayed, which can be obtained combining the time-shift operator with the permanent displacement. The three different kind of motions can be used in turn for the construction of more complicated seafloor motions.

Introducing the time-shift operator:

$$T_\tau f(t) = f(t - \tau) \tag{B1}$$

the simpler elastic seafloor motion (rise and fall) $\eta_e(t)$ is:

$$\eta_e = (1 - T_\tau)\eta_p \tag{B2}$$

where $\eta_p(t)$ is the function describing the permanent seafloor motion. From equation eq. (A12) of Appendix A the free-surface solution at fixed observing point is:

$$\xi(x, t) = F^{-1} I(k, \omega) F \eta(x, t) = H\eta(x, t) \tag{B3}$$

where:

$$I(k, \omega) = -\frac{\omega}{g}\frac{B}{\psi} \tag{B4}$$

F is the operator corresponding to direct Laplace and Fourier transforms. Using the properties of the Laplace transform, with some algebra, we can show that the two operators H and T_τ commute:

$$HT_\tau\eta(x, t) = H\eta(x, t - \tau) = F^{-1} I(k, \omega) e^{-\omega\tau} F\eta(x, t) = \xi(x, t - \tau) = T_\tau H\eta(x, t) \tag{B5}$$

Using this property, the free-surface solution ξ_e, corresponding to the elastic seafloor motion described in eq. (B2), can be written as a function of the solution ξ_p corresponding to permanent displacement:

$$\xi_e = H\eta_e = H(1 - T_\tau)\eta_p = (1 - T_\tau)H\eta_p = (1 - T_\tau)\xi_p \tag{B6}$$

The same conclusion can be easily extended to more complicated bottom motions. Eq. (B6) can be inverted using Laplace transform:

$$\tilde{\xi}_p(x, \omega) = \frac{1}{1 - e^{-\omega\tau}} \tilde{\xi}_e(x, \omega) \tag{B7}$$

where the tilde denotes the Laplace transformed function with respect to t. If the parameter τ is known (for instance from the seismic network), then equation (B7) can be solved and, as in the case of the permanent displacement, the information ξ_p on the source motion can be estimated.

Acknowledgments. This work has been done within the framework of NEAREST EC Project, Contract n. GOCE 037110. The authors thank dr. Paolo Favali and dr. Carlo Lari for the helpful discussions and suggestions.

References

Baptista, M., J. Miranda, F. Chierici, and N. Zitellini (2003), New study of the 1755 earthquake source based on multi-channel seismic survey data and tsunami modelling, *Natural Hazards and Earth System Sciences*, *3*, 333–340.

Boschi, E., E. Guidoboni, G. Ferrari, G. Valensise, and P. Gasperini (Eds.) (1997), *Catalogue of the strong earthquakes in Italy from 461 BC to 1990*, 973 pp., ING & SGA, Bologna.

Comer, R. (1984), The tsunami mode of a flat earth and its excitation by earthquake sources, *Geophys. J. R. astr. Soc.*, *77*, 1–27.

DART project , DART web site: http://nctr.pmel.noaa.gov/dart/index.html.

DONET project , Donet web site: http://www.jamstec.go.jp/jamstec-e/maritec/donet/.

GITEWS project , GITEWS web site: http://www.gitews.org/.

Gu, Z., and H. Wang (1991), Gravity waves over porous bottoms, *Coastal Engineering*, *15*, 497–524.

Habel, F., and C. Bagtzoglou (2005), Wave induced flow and transport in sediment beds, *Journal of the American Water Resources Association*, *41(2)*, 461–476.

Kajiura, K. (1970), Tsunami source, energy and the directivity of wave radiation, *Bull. Earthq. Res. Inst. Tokyo Univ.*, *48*, 835–869.

Kowalik, Z., W. Knight, T. Logan, and P. Whitmore (2005), Numerical modeling of the global tsunami: Indonesian tsunami of 26 december 2004, *Sci. Tsunami Hazard*, *23(1)*, 40–56.

Lomnitz, C., and S. Nilsen-Hofseth (2005), The indian ocean disaster: Tsunami physics and early warning dilemmas, *EOS Trans. AGU*, *86*, 65–70.

Ma, K., H. Kanamori, and K. Satake (1997), Mechanism of the 1975 Kalapana, Hawaii, earthquake inferred from tsunami data, *J. Geophys. Res.*, *104*, 13153–13167.

Merrifield, M., et al. (2005), Tide gauge observations of the indian ocean tsunami, december 26, 2004, *Geophys. Res. Lett.*, *32*, L09,603.

Miyoshi, H. (1954), Generation of the tsunami in compressible water (Part I), *J. Oceanogr. Soc. Japan*, *10*, 1–9.

NEAREST project , NEAREST web site: http://nearest.bo.ismar.cnr.it/.

NGDC Tsunami Catalog , NGDC tsunami catalog web site: http://www.ngdc.noaa.gov/hazard/tsu_db.shtml.

Nosov, M., S. Kolesov, A. Denisova, A. Alekseev, and B. Levin (2007), On the near-bottom pressure variations in the region of the 2003 Tokachi-Oki tsunami source, *Oceanology*, pp. 26–32.

Nosov, M. A. (1999), Tsunami generation in compressible ocean, *Phys. Chem. Earth (B)*, *24*(5), 437–441.

Nosov, M. A., and S. V. Kolesov (2007), Elastic oscillations of water column in the 2003 tokachi-oki tsunami source: in-situ measurements and 3-D numerical modelling, *Nat. Hazards Earth Syst. Sci.*, *7*, 243–249.

Nosov, M. A., and S. N. Skachko (2001), Nonlinear tsunami generation mechanism, *Nat. Hazards Earth Syst. Sci.*, *1*, 251–253.

Nosov, M. A., and S. N. Skachko (2002), Nonlinear mechanism of tsunami generation in a compressible ocean, in *Local Tsunami Warning and Mitigation*, edited by B. W. Levin and M. A. Nosov, pp. 107–114, Janus, Moscow.

Ohmachi, T., H. Tsukiyama, and H. Matsumoto (2001), Simulation of tsunami induced by dynamic displacement of seabed due to seismic faulting, *Bull. Seismological Soc. Am.*, *91*(6), 1898–1909.

Okal, E. A. (1988), Seismic parameters controlling far-field tsunami amplitudes: a review, *Natural Hazards*, *1*, 67–96.

Panza, G., F. Romanelli, and T. Yanovskaya (2000), Synthetic tsunami mareograms for realistic oceanic models, *Geophysical Journal International*, *141*, 498–508.

Sells, C. C. L. (1965), The effect of a sudden change of shape of the bottom of a slightly compressed ocean, *Phil. Trans. Roy. Soc. London (A)*, *258*, 495–528.

Synolakis, C. (1995), Tsunami prediction, *Science*, *270*(15).

Synolakis, C., P. Liu, G. Carrier, and H. Yeh (1997), Tsunamigenic sea-floor deformation, *Science*, *278*, 598–600.

Synolakis, C., J. Bardet, J. Borrero, H. Davies, E. Okal, E. Silver, J. Sweet, and D. Tappin (2002), Slump origin of the 1998 Papua New Guinea tsunami, *Proceedings of the Royal Society of London A*, *458*, 763–769.

Tinti, S., A. Maramai, and L. Graziani (2004), The new catalogue of italian tsunamis, *Natural Hazards*, *33*, 439–465.

Titov, V. V., A. B. Rabinovich, H. O. Mofjeld, R. I. Thomson, and F. Gonzalez (2005), The global reach of the 26 December 2004 Sumatra tsunami, *Science*, *309*, 2045–2048.

TRANSFER project , TRANSFER web site: http://www.transferproject.eu/.

Ward, S. (1980), Relationships of tsunami generation and an earthquake source,, *J. Phys. Earth*, *28*, 441–474.

Ward, S. (1981), On tsunami nucleation: I. a point source, *J. Geophys. Res.*, *86*, 7895–7900.

Ward, S. (1982), On tsunami nucleation: II. an instantaneous modulated line source, *Phys. Earth Planet. Inter.*, *27*, 273–285.

Zitellini, N., F. Chierici, R. Sartori, and L. Torelli (1999), The tectonic source of the 1755 Lisbon earthquake and tsunami, *Annali di Geofisica*, *42*, 49–55.

Figure 1. The acoustic modulation and tsunami: free surface plot at 100km (a), 200km (b), 300km (c) and 1000km (d) distance from the source respectively. The parameters of the simulation are: amplitude of the bottom displacement $\eta_0 = 1$m, duration of motion $\tau = 25$ second. The source length is $2a = 60$ km and the water depth is $h = 3000$m, the porous sea bed thickness is 1500 m, with volumetric porosity $n = 0.3$ and a permeability $K_p = 10^{-6}\text{cm}^2$.

Figure 2. Inset (a), (b) and (c): the same plots of corresponding inset in figure 1, except for the depth of the observing point, here chosen at 1500m depth. The acoustic modulation is similar to the one plotted at the free surface, but distorted by the factor $f_p(k, \omega)$ described in the appendix A. The tsunami is indicated by the arrows. The inset (d) shows a relevant amplitude of the acoustic signal at a 1000 km distance from the source.

Figure 3. The acoustic modulation due to different source length a of 30km, 60km and 90km respectively for inset (a), (b), and (c).The observing distance is 300km and the water layer is 1500m deep. The sedimentary bottom has a thickness of 750m, the motion duration is 1 second (bottom motion amplitude, permeability and porosity are the same as in previous simulations). As can be easily noticed by the zoomed envelopes of inset (d) the number of pulses in same time interval varies with the source length, scaling with the ratio among the lengths. Inset (e): the mean slope of the pulses varies with the energy released in the water column by the sources of different length and vary with the ratio among the source lengths $2a$.

Figure 4. The inset (a), (b), (c) show the acoustic modulation, with the envelopes superposed, due to different source velocities. Inset (d) shows the comparison among the envelopes, with the value of the mean slope of the pulses. The mean slopes variation is directly proportional to the velocities variation. As in figure 3 the mean slope is an indicator of the energy released into the water by the ground motion, but differently from there the number of pulses is the same within the same time interval. The length of the source is $2a = 30$ km. The observation point is located at distance 300 km from the source and all the other parameters, such as water depth, porosity etc. are the same of Figure 3.

Figure 5. The envelopes of permanent displacement motions with periods 4, 8, 12 and 16 seconds are respectively shown in inset (a), (b), (c) and (d). Here the water depth is 1500m, the sediment thickness is 750m, the source length is 30km and the observation point is at 375km from the source. All the other parameters are the same of figure 3. The interference between the sea floor motion frequency and the water layer fundamental frequency of oscillation brings to a very different modulation pattern with respect to the one caused by same sea floor motion with frequencies far from the water layer fundamental frequency. Moreover the modulation amplitude is smaller.

Figure 6. As can be noticed by the inset on the left, different "resonant" period choices for sea floor motion produce similar envelopes, which in the first pulses scale in amplitude with the period (i.e. inverse of bottom velocities) and then flatten on tails of equal amplitudes before the tsunami arrival (about 3100 seconds in this simulation). Right inset: mean slopes against "resonant" bottom motion periods The linear trend is clearly recognizable; the correlation coefficient is $r^2 = 0.9987$.

Figure 7. The acoustic modulation produced by a bottom motion with period far from resonance is shown for pattern comparison with respect to Fig 5 (the observation point is placed at same distance of 375km from the source).

Figure 8. The amplitude spectrum corresponding to fig.5b (”resonant” bottom motion period of 8 seconds) and its zoomed sketch, boxes (a) and (b) respectively. In inset (c) and (d) the amplitude spectrum and zoomed sketch are shown for a bottom motion of period 10 seconds, far from the resonance (the other parameters are the same). Note the different spectral distribution and amplitudes.

Figure 9. The tsunami generated by a 4 sec period ”resonant” permanent displacement, the observation point is at $\bar{x}$ =100km distance from the source. The tsunami amplitude is the same as in Fig.1.

Figure 10. Comparison of tsunami generation process with (black line) or without (red line) a porous layer. Inset (a): tsunami profile at fixed time t=100 s after the initial bottom motion; green dotted lines delimit the bottom motion area. Inset (b): free surface signals at 800 km distance from the source. Inset (c) and (d): amplitude spectrum corresponding to inset (b) and its zoomed sketch. The effect of the porosity is a lowering of the acoustic modulation and tsunami amplitude and a frequency smoothing. The frequency cut off due to the action of porosity is clearly shown. The sediment layer is 1800 m thick and the porosity is chosen as $n = 0.5$. The motion duration is 20 second and the source extension is $2a = 30$ km.

Figure 11. Some ”basic ” kind of motion are shown: on the left the time history and on the right corresponding piston motions.

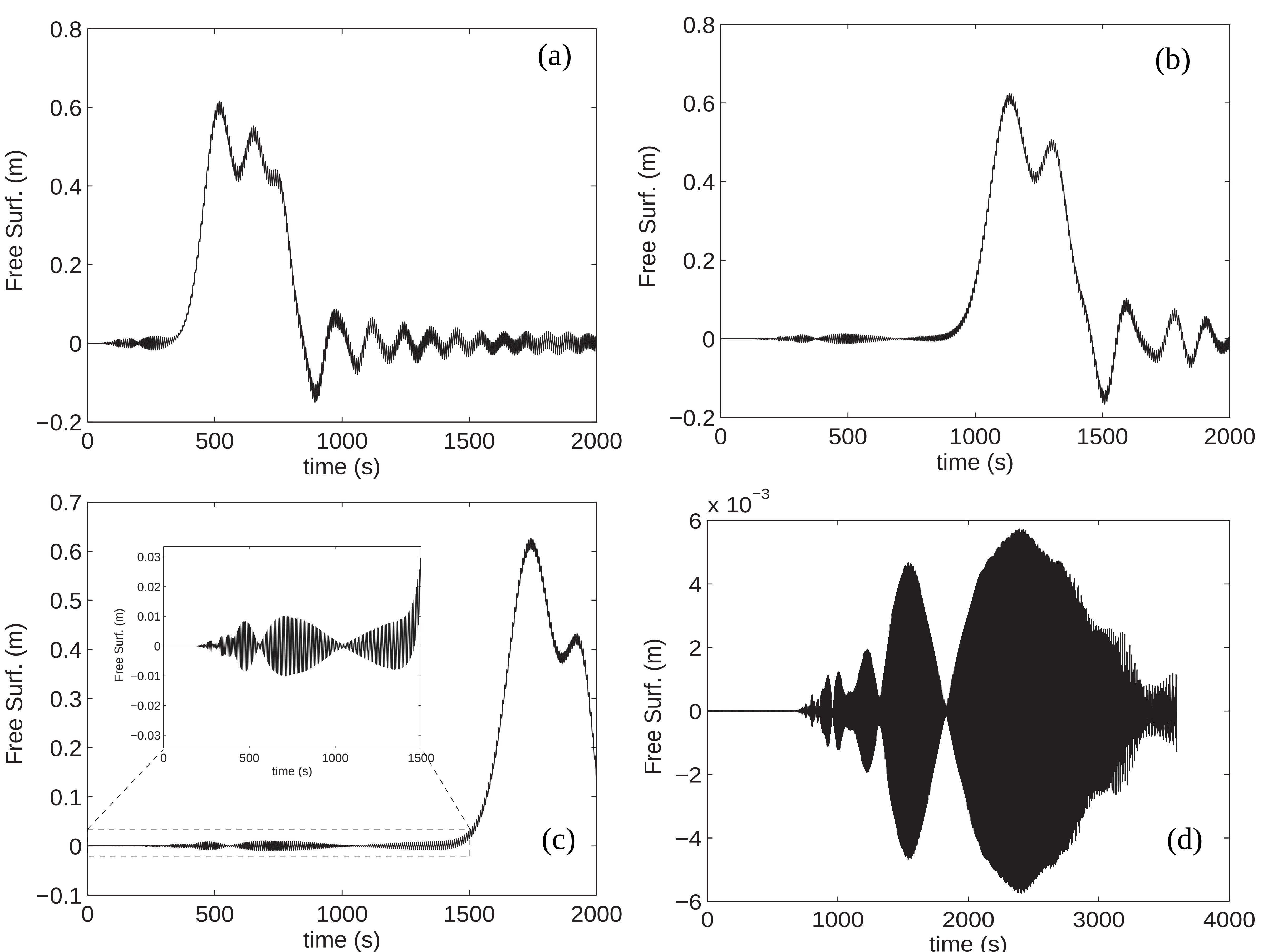

(a)
(b)
(c)
(d)
Free Surf. (m)
time (s)
x 10^-3

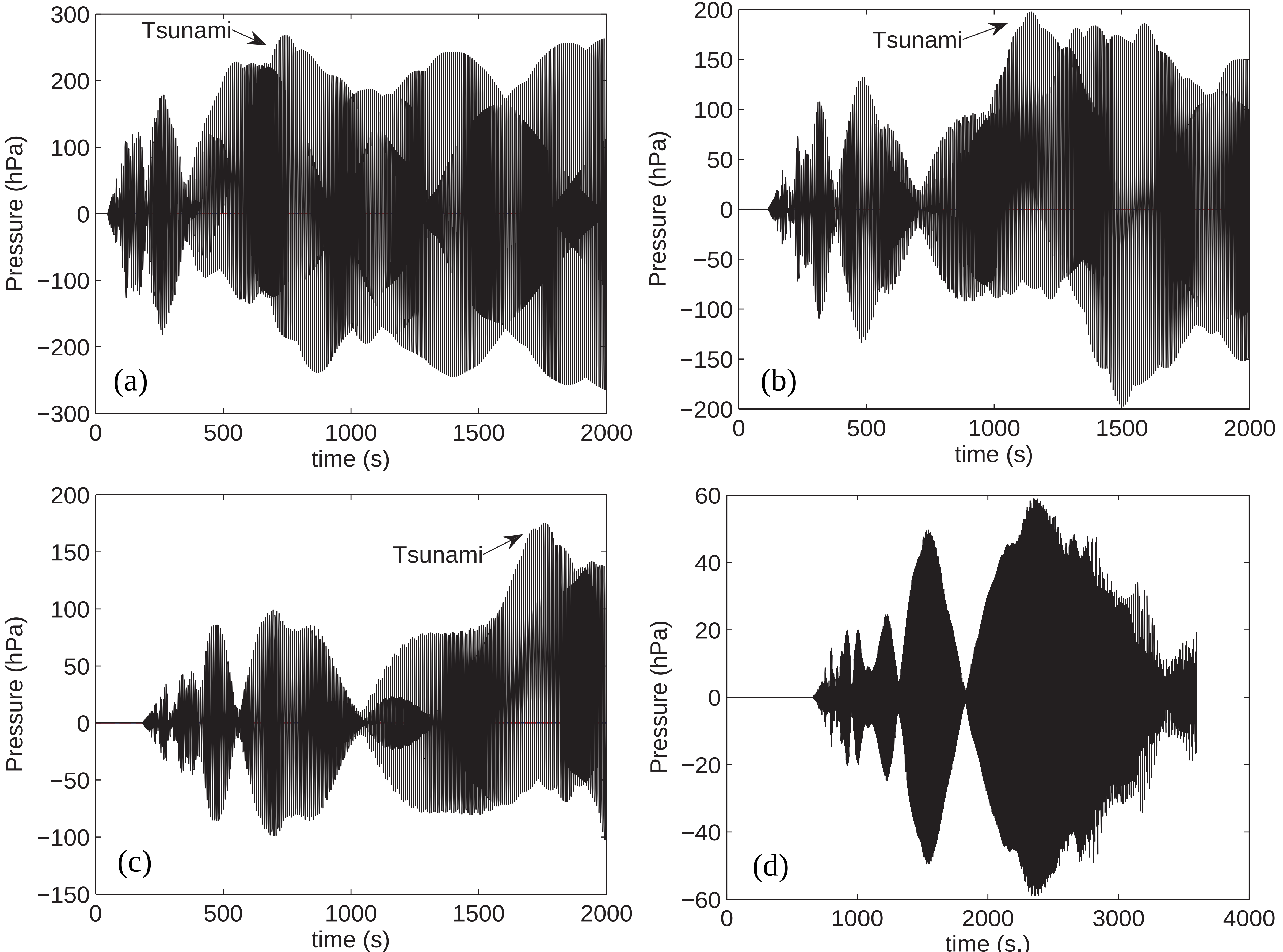

Tsunami
Pressure (hPa)
time (s)
(a)
Tsunami
Pressure (hPa)
time (s)
(b)
Tsunami
Pressure (hPa)
time (s)
(c)
Pressure (hPa)
time (s.)
(d)

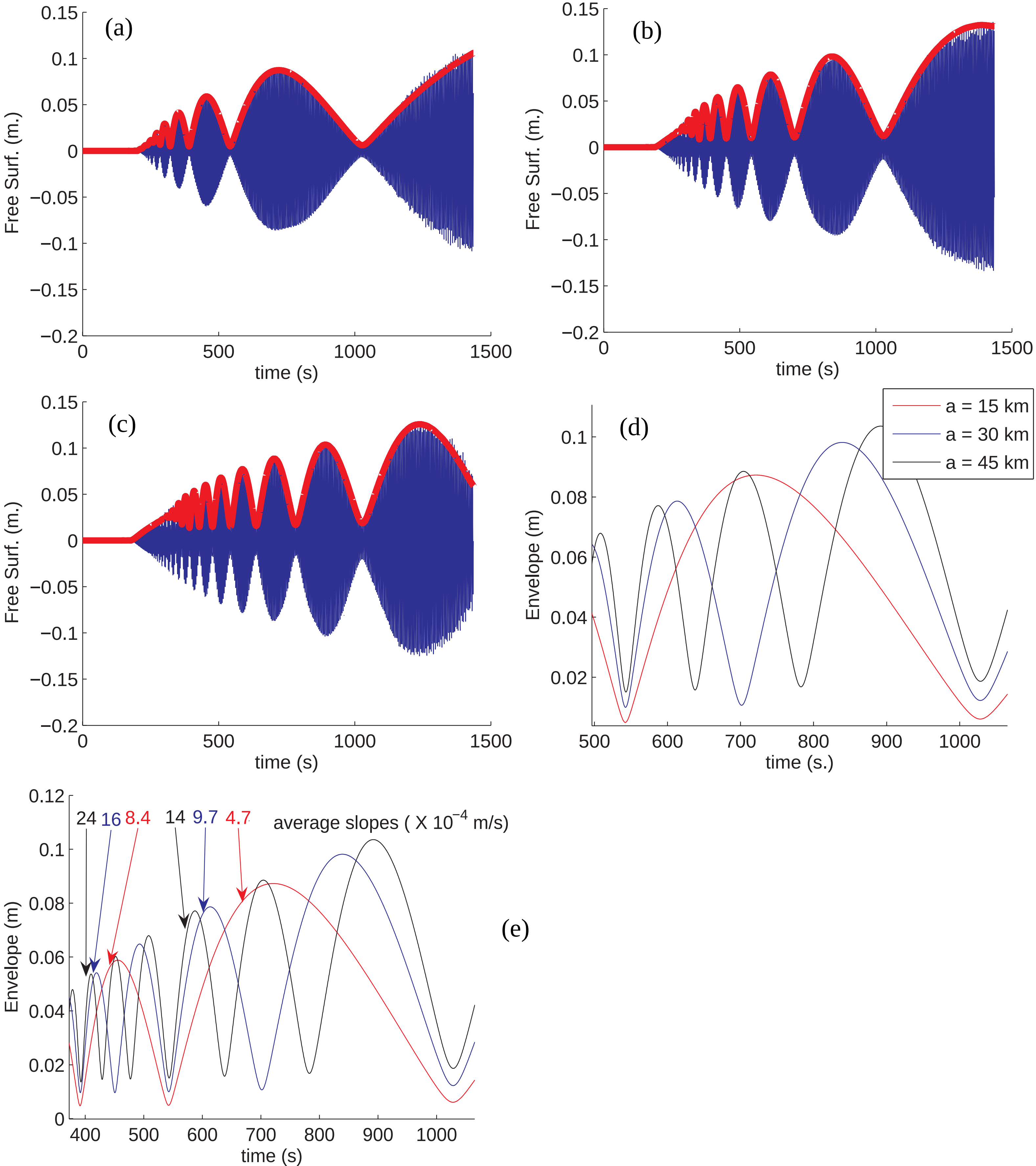

(a)
(b)
(c)
(d)
(e)
Free Surf. (m.)
time (s)
Envelope (m)
time (s.)
a = 15 km
a = 30 km
a = 45 km
24
16
8.4
14
9.7
4.7
average slopes (X 10^{-4} m/s)

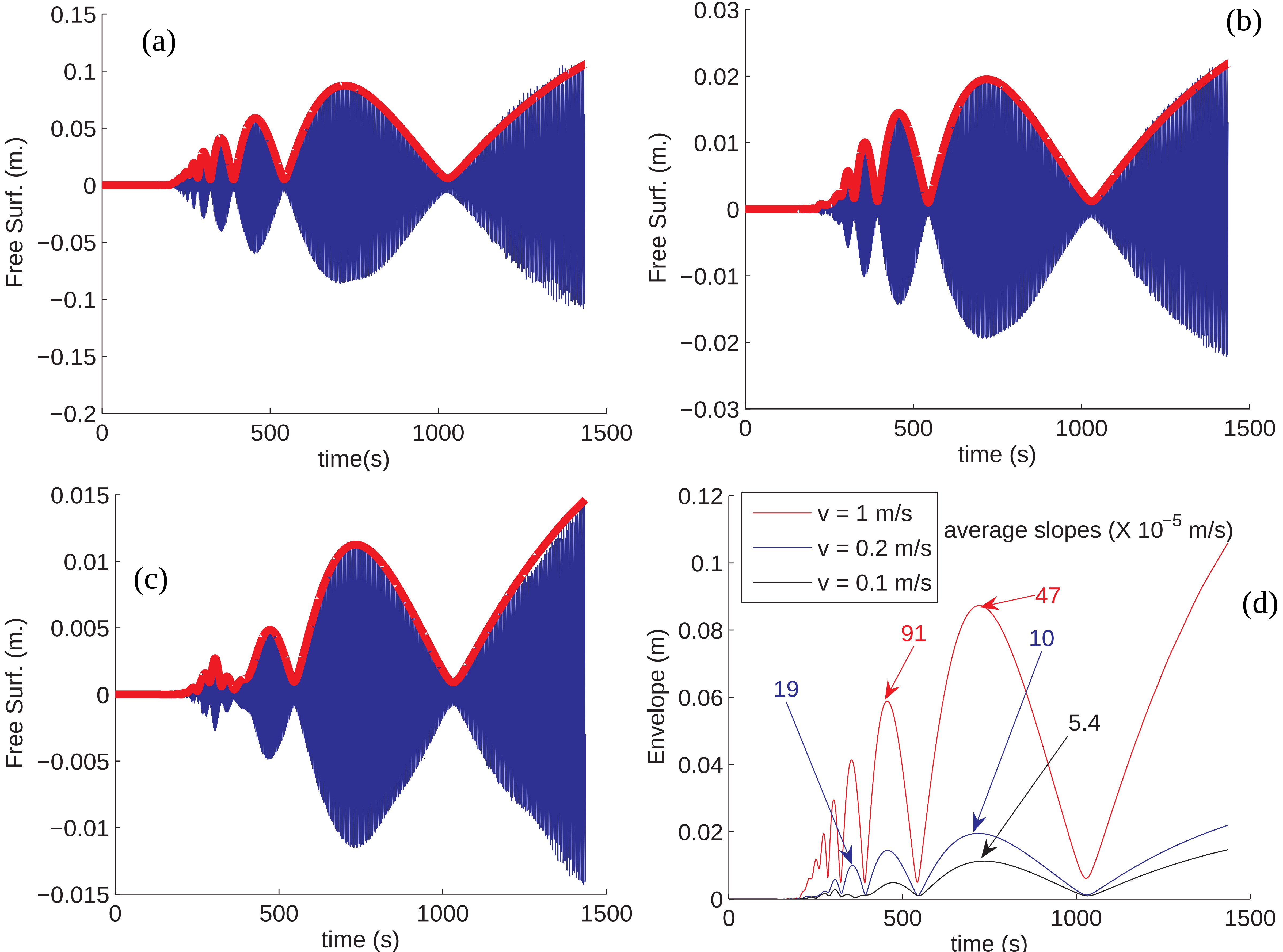

(a)
Free Surf. (m.)
time(s)
(b)
Free Surf. (m.)
time (s)
(c)
Free Surf. (m.)
time (s)
(d)
Envelope (m)
time (s)
v = 1 m/s
v = 0.2 m/s
v = 0.1 m/s
average slopes (X 10^{-5} m/s)
47
91
10
19
5.4

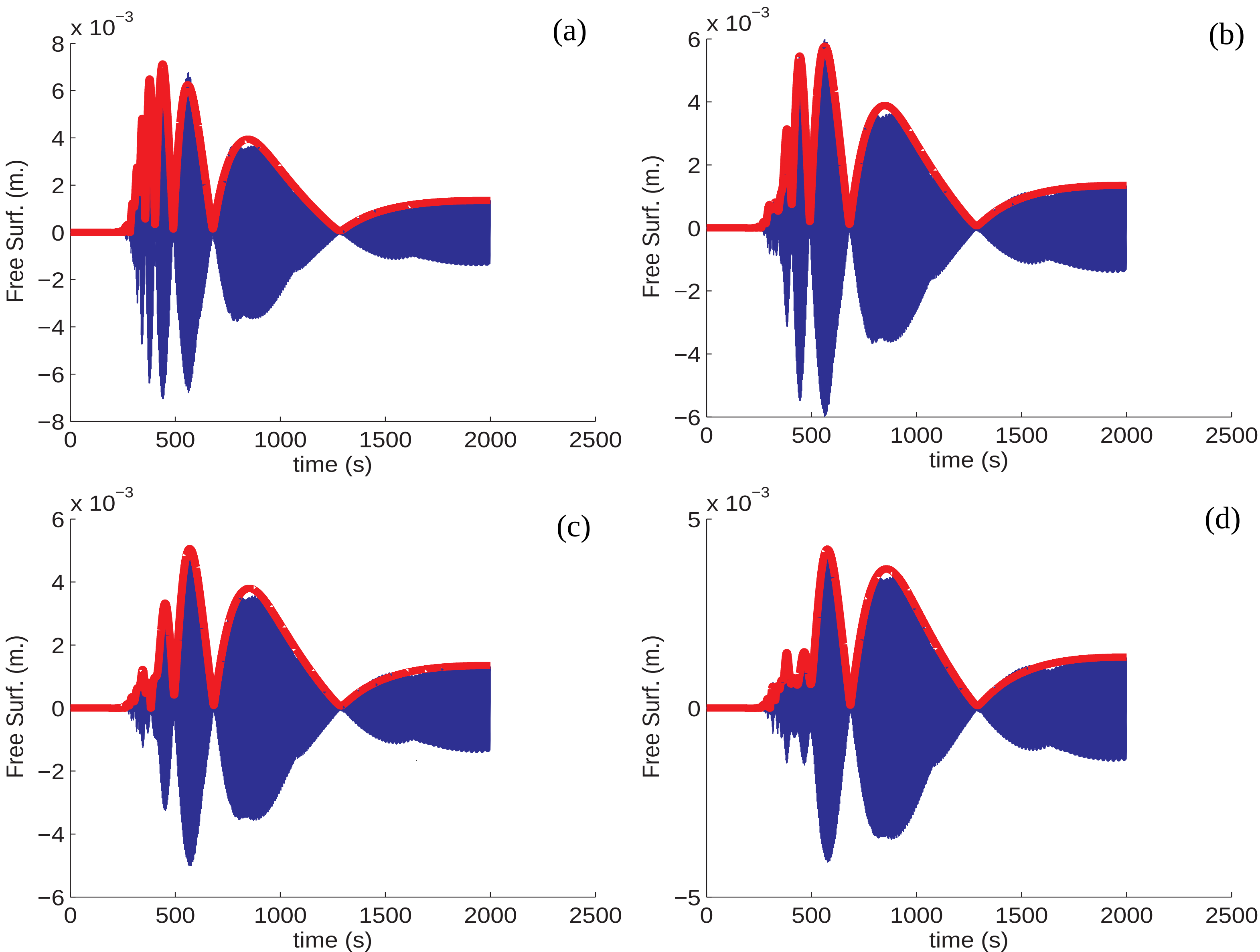

(a)
(b)
(c)
(d)
x 10^−3
Free Surf. (m.)
time (s)
0
500
1000
1500
2000
2500

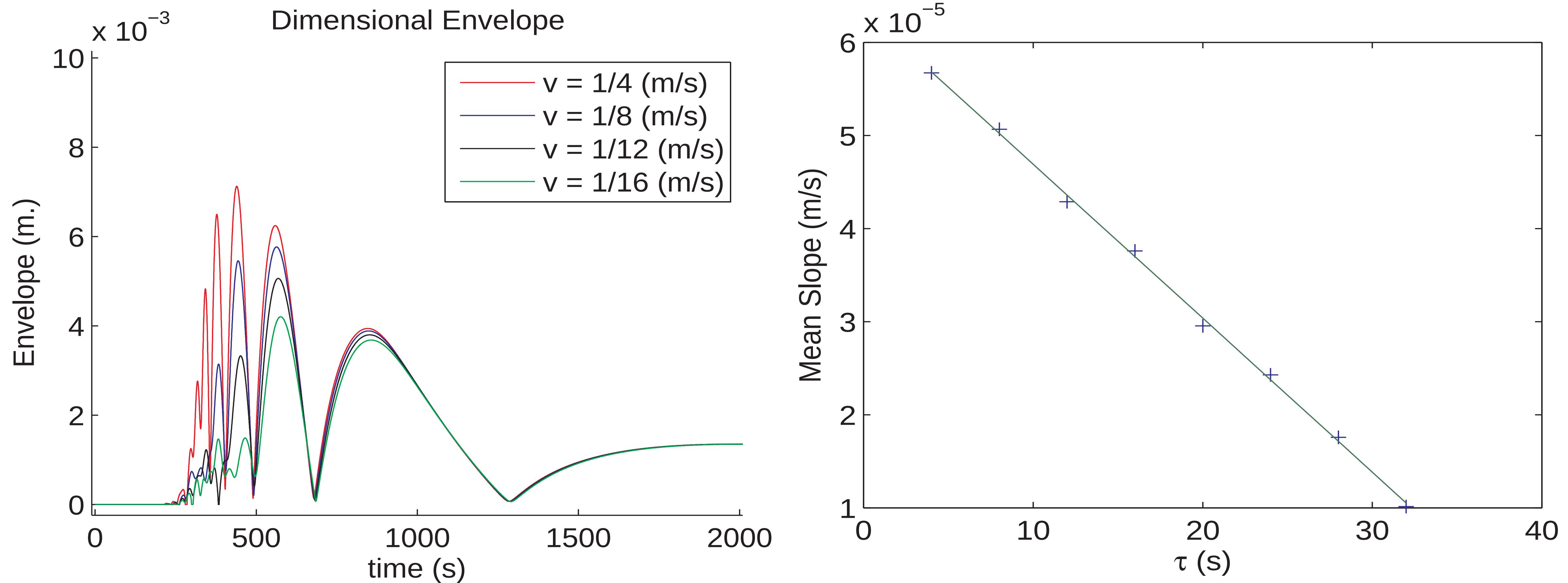

Dimensional Envelope
x 10^−3
10
8
6
4
2
0
Envelope (m.)
v = 1/4 (m/s)
v = 1/8 (m/s)
v = 1/12 (m/s)
v = 1/16 (m/s)
0
500
1000
1500
2000
time (s)
x 10^−5
6
5
4
3
2
1
Mean Slope (m/s)
0
10
20
30
40
τ (s)

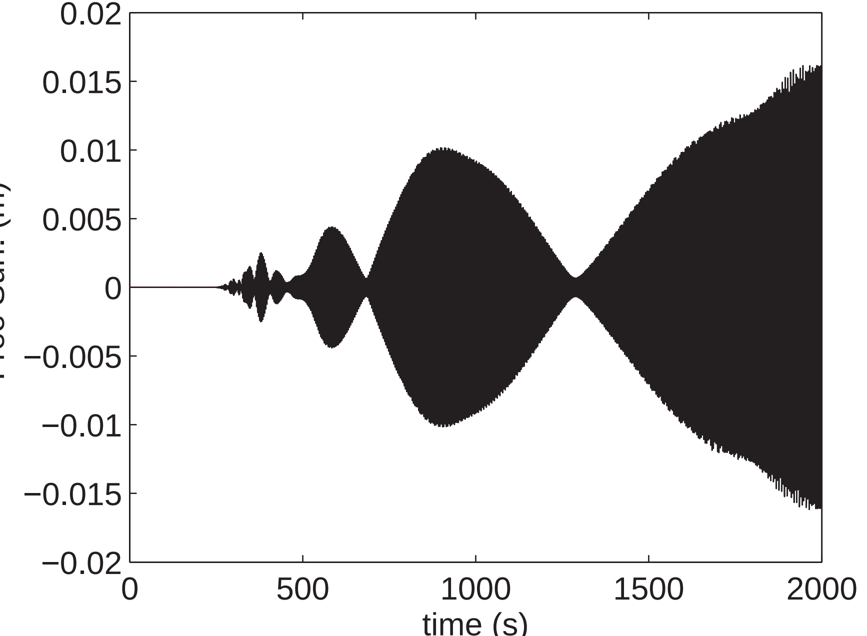
0.02
0.015
0.01
0.005
0
−0.005
−0.01
−0.015
−0.02
0
500
1000
1500
2000
time (s)

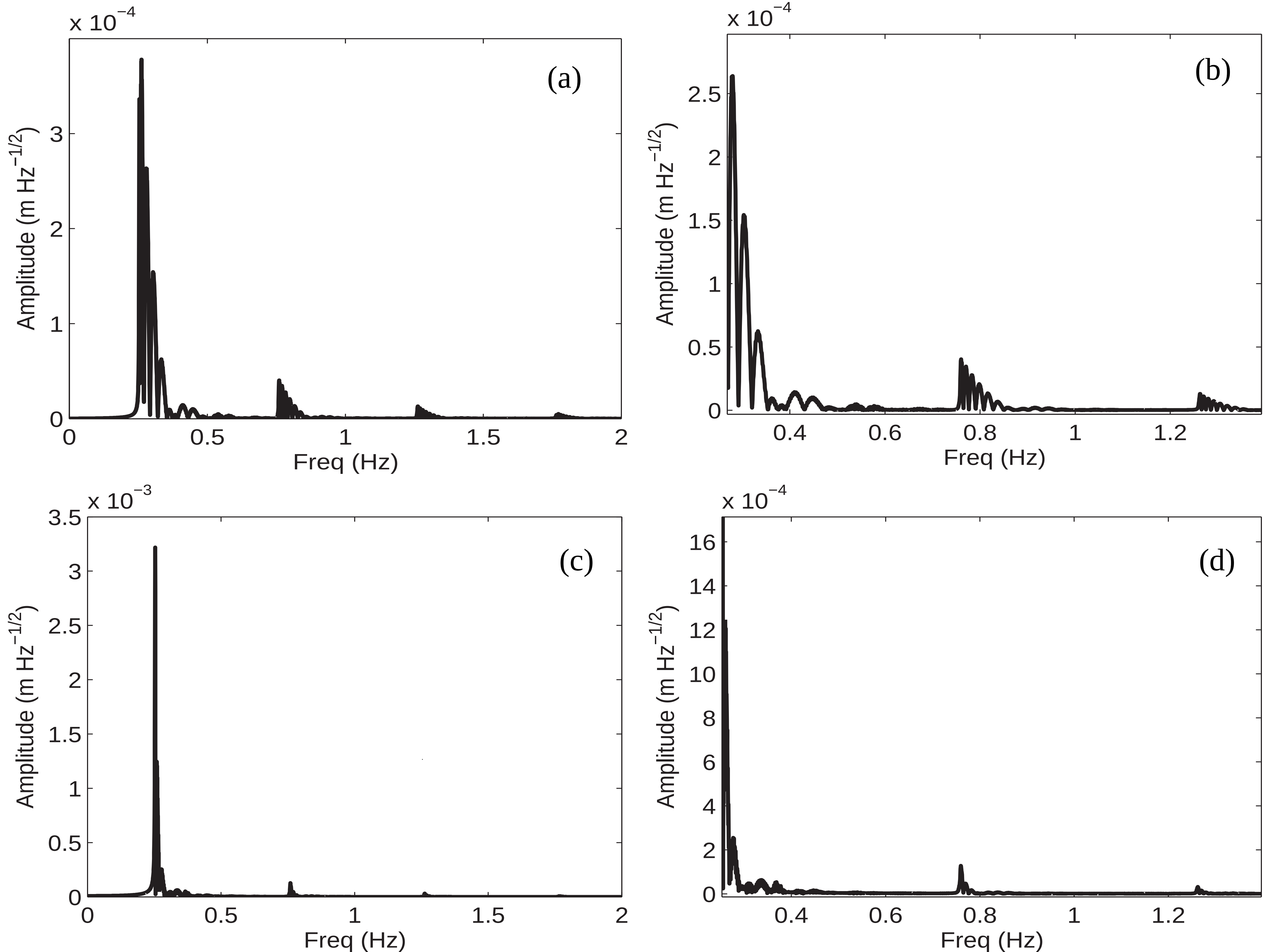

x 10^−4
(a)
Amplitude (m Hz^−1/2)
Freq (Hz)
x 10^−4
(b)
Amplitude (m Hz^−1/2)
Freq (Hz)
x 10^−3
(c)
Amplitude (m Hz^−1/2)
Freq (Hz)
x 10^−4
(d)
Amplitude (m Hz^−1/2)
Freq (Hz)

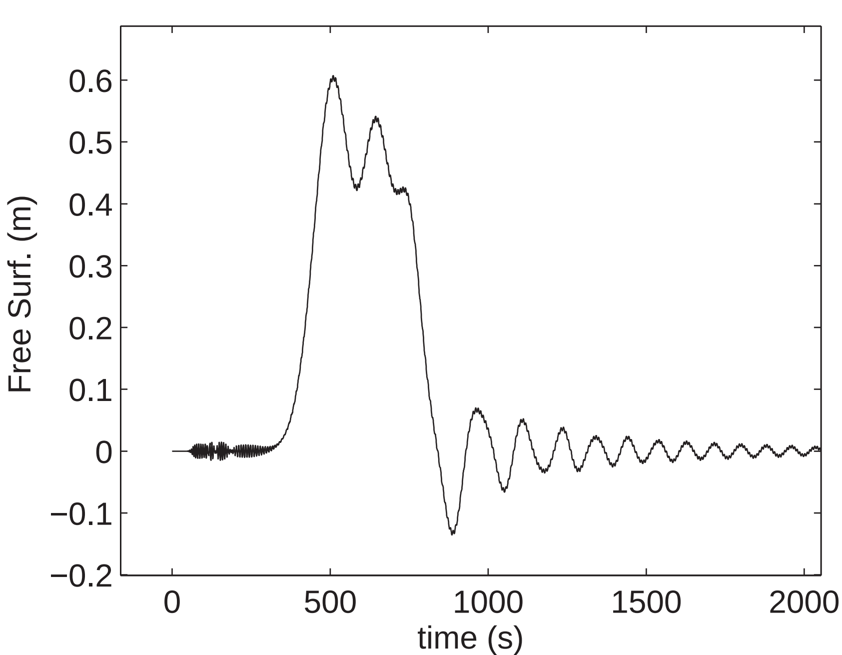
Free Surf. (m)
time (s)
0.6
0.5
0.4
0.3
0.2
0.1
0
−0.1
−0.2
0
500
1000
1500
2000

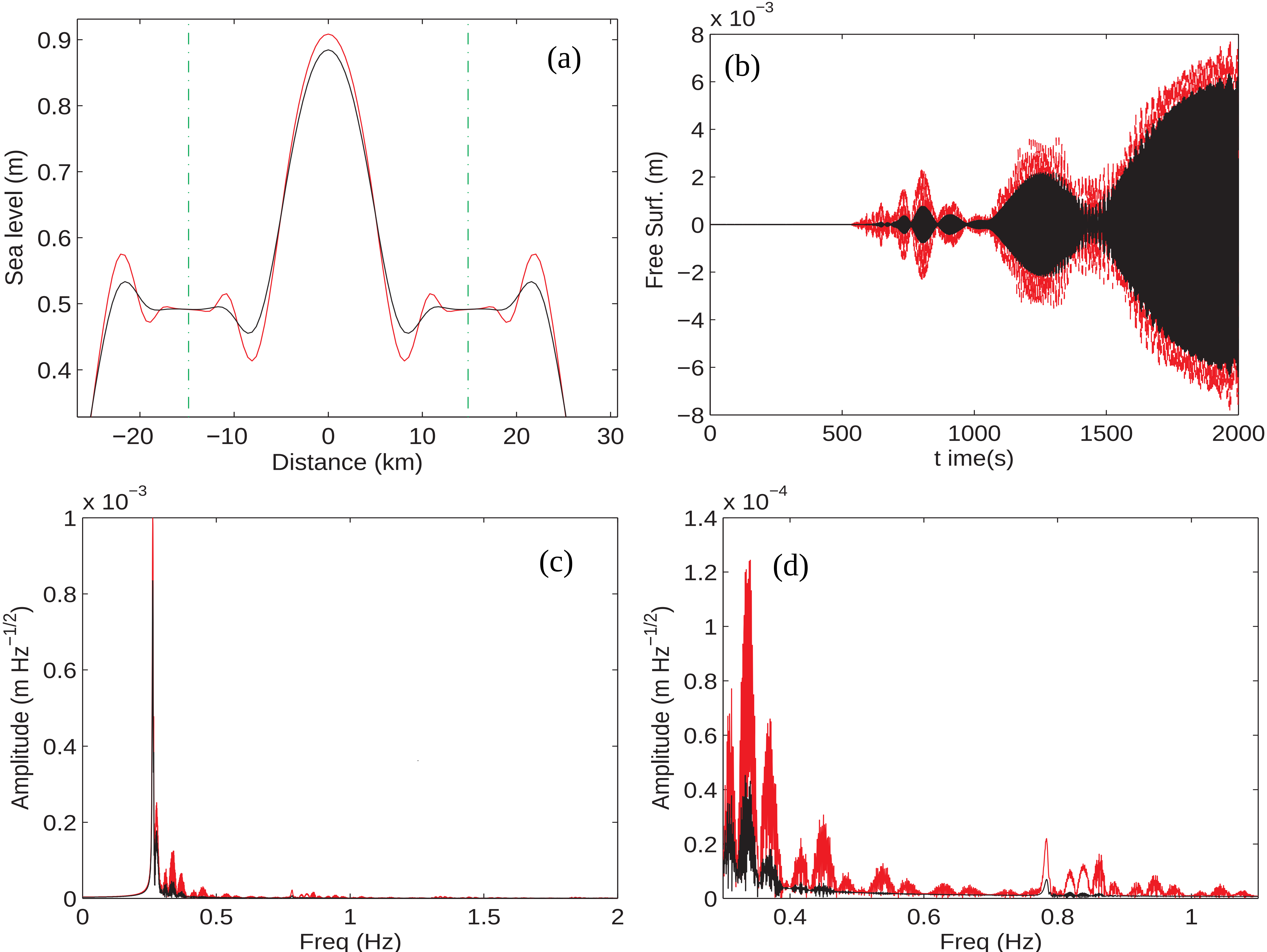

(a)
Sea level (m)
0.9
0.8
0.7
0.6
0.5
0.4
−20
−10
0
10
20
30
Distance (km)
(b)
x 10^−3
8
6
4
2
0
−2
−4
−6
−8
Free Surf. (m)
0
500
1000
1500
2000
t ime(s)
(c)
x 10^−3
1
0.8
0.6
0.4
0.2
0
Amplitude (m Hz^−1/2)
0
0.5
1
1.5
2
Freq (Hz)
(d)
x 10^−4
1.4
1.2
1
0.8
0.6
0.4
0.2
0
Amplitude (m Hz^−1/2)
0.4
0.6
0.8
1
Freq (Hz)

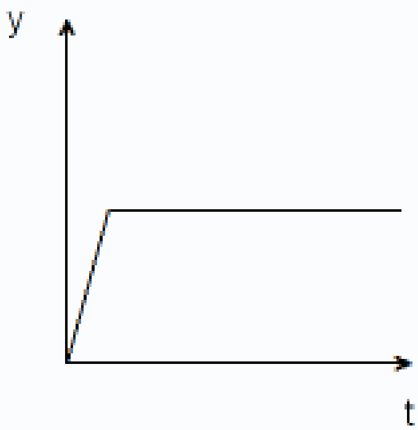
y
t

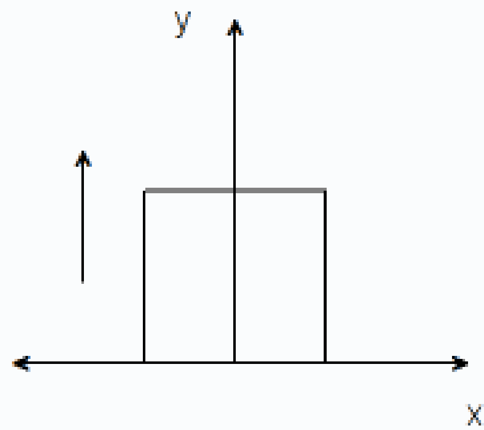
y
x

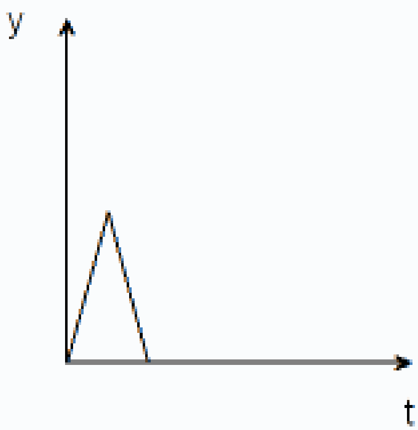
y
t

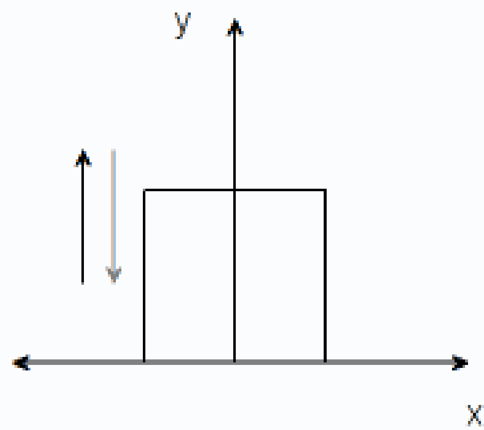
y
x

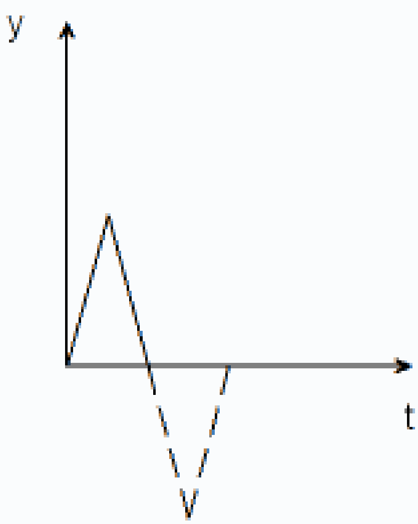
y
t

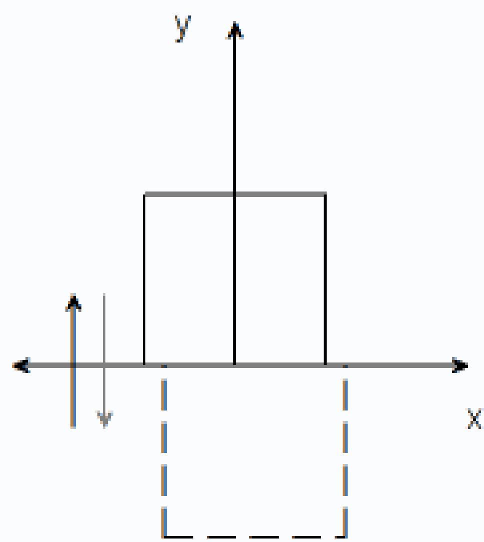
y
x